



OPEN ACCESS

EDITED BY

Marco La Torre,
Sapienza University of Rome,
Italy

REVIEWED BY

Xiaowei Han,
Nanjing Drum Tower Hospital,
China Tao Zheng,
First Hospital of Qinhuangdao,
China

*CORRESPONDENCE

Zhikui Chen
jimchen2003@163.com

[†]These authors have contributed
equally to this work and share
first authorship

SPECIALTY SECTION

This article was submitted to
Gastrointestinal Cancers:
Colorectal Cancer,
a section of the journal
Frontiers in Oncology

RECEIVED 26 March 2022

ACCEPTED 09 August 2022

PUBLISHED 26 August 2022

CITATION

Zhuo M, Guo J, Tang Y, Tang X,
Qian Q and Chen Z (2022) Ultrasound
radiomics model-based nomogram for
predicting the risk Stratification of
gastrointestinal stromal tumors.
Front. Oncol. 12:905036.
doi: 10.3389/fonc.2022.905036

COPYRIGHT

© 2022 Zhuo, Guo, Tang, Tang, Qian
and Chen. This is an open-access article
distributed under the terms of the
Creative Commons Attribution License
(CC BY). The use, distribution or
reproduction in other forums is
permitted, provided the original
author(s) and the copyright owner(s)
are credited and that the original
publication in this journal is cited, in
accordance with accepted academic
practice. No use, distribution or
reproduction is permitted which does
not comply with these terms.

Ultrasound radiomics model-based nomogram for predicting the risk Stratification of gastrointestinal stromal tumors

Minling Zhuo[†], Jingjing Guo[†], Yi Tang, Xiubin Tang,
Qingfu Qian and Zhikui Chen*

Department of Ultrasound, Fujian Medical University Affiliated Union Hospital, Fuzhou, China

This study aimed to develop and evaluate a nomogram based on an ultrasound radiomics model to predict the risk grade of gastrointestinal stromal tumors (GISTs). 216 GIST patients pathologically diagnosed between December 2016 and December 2021 were reviewed and divided into a training cohort (n = 163) and a validation cohort (n = 53) in a ratio of 3:1. The tumor region of interest was depicted on each patient's ultrasound image using ITK-SNAP, and the radiomics features were extracted. By filtering unstable features and using Spearman's correlation analysis, and the least absolute shrinkage and selection operator algorithm, a radiomics score was derived to predict the malignant potential of GISTs. a radiomics nomogram that combines the radiomics score and clinical ultrasound predictors was constructed and assessed in terms of calibration, discrimination, and clinical usefulness. The radiomics score from ultrasound images was significantly associated with the malignant potential of GISTs. The radiomics nomogram was superior to the clinical ultrasound nomogram and the radiomics score, and it achieved an AUC of 0.90 in the validation cohort. Based on the decision curve analysis, the radiomics nomogram was found to be more clinically significant and useful. A nomogram consisting of radiomics score and the maximum tumor diameter demonstrated the highest accuracy in the prediction of risk grade in GISTs. The outcomes of our study provide vital insights for important preoperative clinical decisions.

KEYWORDS

gastrointestinal stromal tumors, radiomics, ultrasound, risk grade, model, nomogram

Introduction

Gastrointestinal stromal tumors (GISTs) are the most common mesenchymal-derived tumors of the gastrointestinal tract, with diverse biological behaviors (1, 2). Preoperative prediction of the malignant potential of GISTs is of great significance for clinical treatment and prognostic prediction (3, 4). However, the preoperative assessment

of the risk grading of gastrointestinal stromal tumors is difficult because of the difficulty in calculating mitotic counts preoperatively. Therefore, the research on identifying a preoperative diagnostic method that is reproducible and can objectively predict the risk grading of GISTs has recently attracted significant attention in recent years.

The transabdominal ultrasonography, especially medium- and high-frequency ultrasonography, can clearly display the layers of the gastrointestinal wall. It can be easily operated and can be dynamically observed repeatedly. The transabdominal gastrointestinal ultrasonography is a commonly used method in preoperative imaging examination of GIST. Although transabdominal ultrasonography can directly evaluate the tumor size, location, shape, boundary, echo homogeneity, and blood flow signals, which is of great value for tumor detection, as well as the localization and diagnosis, this method was easily affected by examiner's subjective vision and diagnostic experience. Thus, because of tumor heterogeneity, these subjective assessments have relatively low accuracy and repeatability (5, 6). With the development of artificial intelligence, radiomics prediction models have gained attention in cancer diagnosis (7–10). Radiomics can extract inaccessible feature data from medical images with a high-throughput and has great application prospects in predicting the biological behavior of tumors (11, 12).

In recent years, some studies have explored the value of radiomics based on computed tomography or magnetic resonance imaging to predict the malignant potential of GISTs (13, 14); however, the application value of ultrasound has not been reported. In this study, accessible and universal ultrasound images were selected as the basic imaging data, and the internal characteristic information of the tumors was extracted. In order to integrate radiomics features, clinical factors, and conventional ultrasound features to adequately evaluate and effectively support preoperative clinical management, we aimed to construct a radiomics nomogram to predict the risk grade of GISTs in this study.

Materials and methods

Study population

This retrospective study was approved by the ethics committee of Fujian Medical University Affiliated Union Hospital. The signed informed consent forms were waived. From December 2016 and December 2021, 368 GIST patients histologically confirmed at our institution were retrospectively recruited. The inclusion criteria were as follows: 1) the diagnosis of GISTs was confirmed by postoperative pathology, 2) the patients performed ultrasonic examination within 15 days before operation, and 3) the ultrasound image clearly showed the target lesion. The excluding standards were as follows: 1)

patient received other preoperative treatment such as imatinib or other tyrosine kinase inhibitors and 2) incomplete ultrasound and clinical data. In this study, 216 patients were enrolled (126 men and 90 women; mean age 60 ± 11 years; range 28–86 years) (Figure 1). Patients were divided into a training cohort ($n = 163$; 95 men and 68 women; mean age 60 ± 12 years) and validation cohort ($n = 53$; 31 men and 22 women; mean age 59 ± 11 years) after simple randomization at a ratio of 3:1. According to the pathological results and the National Institutes of Health modified criteria, patients in this study were divided into low-malignant potential (very low to low risk) and high-malignant potential (intermediate to high risk) groups.

Clinical characteristics

Preoperative demographic and clinicopathological data of the 216 GIST patients were collected, including age, gender, height, weight, tumor location (stomach or extragastric), and tumor size (maximum diameter). In addition, this study collected postoperative data, including the risk of NIH stratification and growth patterns.

Radiomics analysis process

Research on radiomics mainly includes the following steps: tumor segmentation, image processing and feature extraction, feature selection, modeling, and evaluation (Figure 2). In the training cohort, we combined different dimension reduction technologies to establish radiomics models. Finally, the internal validation cohort was used to evaluate the generalization performance of the model.

Ultrasound image acquisition and tumor image segmentation

Color doppler ultrasonic diagnostic apparatus from Toshiba Aplio 500, Supersonic Aixplorer, and PHILIPS EPIQ5 was used. Transabdominal ultrasound was performed using a convex array probe and a line array probe. We conducted a retrospective review of the image data and selected two-dimensional (2D) ultrasound images in digital imaging and communications in medicine (DICOM) format that scanned by convex array probe, which clearly showed the largest cross-section of each lesion. The tumor location (gastric or extra-gastric), internal echo (hypoecho or isoecho), echo homogeneity (homogeneous or inhomogeneous), boundary (clear or unclear), shape (regular or irregular), blood flow signals of the lesion (according to the Alder blood flow classification, where grades 0 and 1 were merged as low blood supply, and grades 2 and 3 were merged as multiple blood supply), presence of necrotic cystic

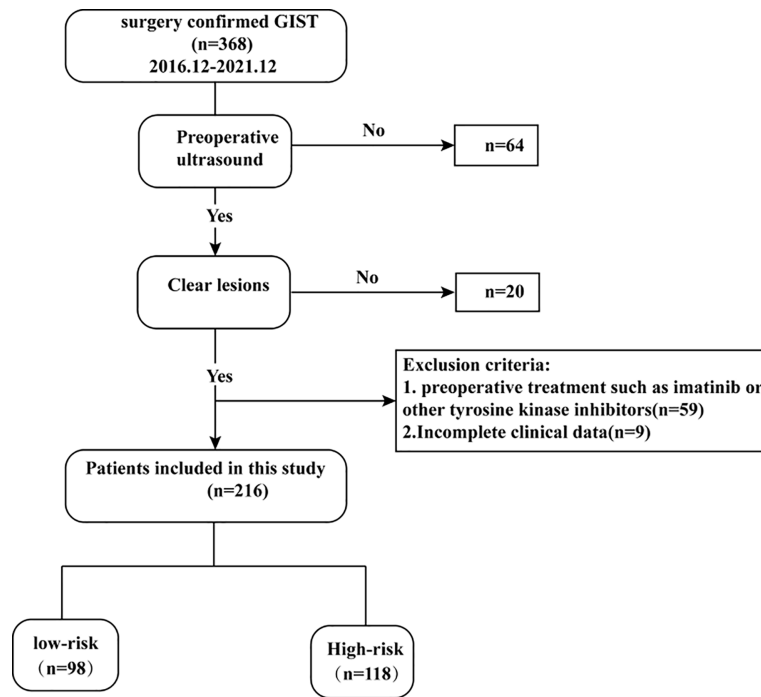


FIGURE 1
Flowchart of inclusion and exclusion of the study population.

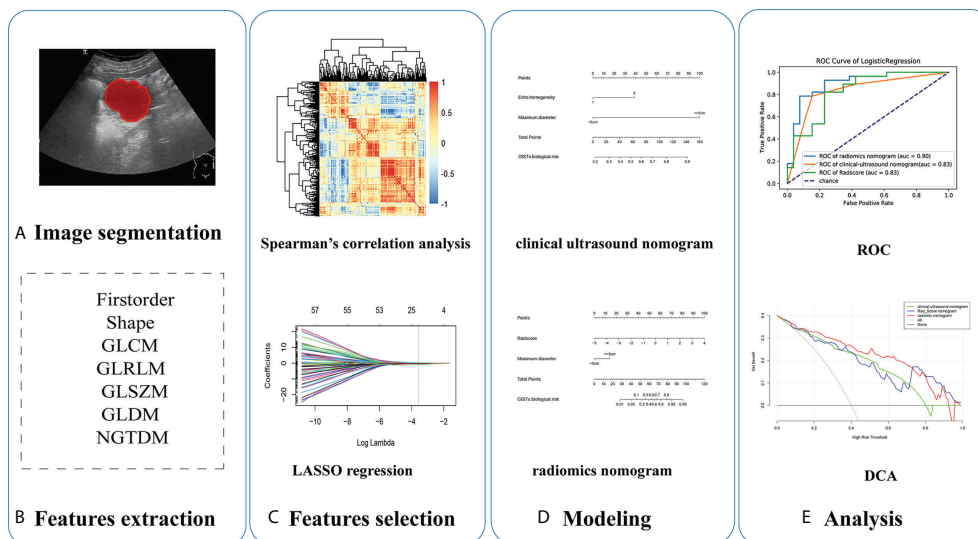


FIGURE 2
Five steps of radiomics research: (A) ultrasound imaging and tumor segmentation, (B) image processing and feature extraction, (C) feature selection, (D) modeling, and (E) performance of models.

degeneration (necrotic areas were diagnosed from sharply demarcated anechoic areas), and maximum lesion diameter (≤ 5.0 cm or >5.0 cm) were recorded in detail.

In this study, the tumor outline at the largest cross-sectional area was manually drawn to indicate the region of interest (ROI) along the tumor margin using a free open-source software package (ITK-SNAP, version 3.8.0, University of Pennsylvania, Philadelphia, USA).

Evaluation of radiomics feature reproducibility

To assess interobserver reliability and intraobserver reproducibility, 30 cases were chosen randomly from the training cohort for ROI delineation and ROI-based feature extraction by two experienced radiologists (radiologist 1 with an experience of 10 years and radiologist 2 with 5 years' experience). Interclass and intraclass correlation coefficients (ICCs) were used to evaluate the agreement of feature extraction. The intraobserver ICC was calculated based on two feature extractions by radiologist 1. The interobserver ICC was calculated based on the features extracted first by radiologist 1 and subsequently by radiologist 2. All radiologists were blinded to the pathology results. There was good agreement when the ICC was greater than 0.75, and features were retained with good repeatability (15).

Radiomics feature extraction and data preprocessing

Because the ultrasound images were collected using three different ultrasound instruments and the feature vectors had a wide range, to eliminate the variance caused by different scanner acquisitions, avoid anisotropic resolution, and improve the reproducibility, we preprocessed the image before feature extraction with the open-source Pyradiomics package (version 2.12; <https://pyradiomics.readthedocs.io/en/2.1.2/>). Images were normalized by centering to the mean standard deviation, resampled to a voxel size using B-Spline interpolation, and gray-level discretized by a fixed bin width of 5 in the histogram.

The radiomics features of the ROI were extracted using the "PyRadiomics" package in Python. The extracted radiomics features were divided into three categories: 2D shape-based features, first-order statistical features, and structural texture features. The structural texture features include five grayscale matrices: gray-level co-occurrence matrix (GLCM), gray-level run-length matrix (GLRLM), gray-level size-zone matrix (GLSZM), gray-level dependence matrix (GLDM), and features of neighborhood gray-tone difference matrix (NGTDM). Furthermore, to extract high-dimensional features from different frequency scales, eight imaging filters

were applied to the raw images: wavelet, square, square root, logarithmic, exponential, gradient, LoG, and local binary pattern (LBP). Finally, 765 quantitative radiomics features were extracted for each patient.

Z-score normalization was used to convert different data to the same order of magnitude, and the calculation formula was as follows: $y=(x-u)/\sigma$, where μ is the mean and σ is the standard deviation. Following the Z-score normalization, the data comparability was improved, demonstrating enhanced robustness for subsequent model building.

Construction of clinical ultrasound nomogram, calculation of the radiomics score (Rad-Score), and construction of radiomics nomogram

Univariate logistic regression was used to screen statistically significant predictors, and multivariate logistic analysis was subsequently performed for the factors that were determined to be statistically significant. The final model was selected by backward stepwise elimination with Akaike information criteria as the stopping rule and a clinical ultrasound nomogram was constructed (16).

The R software (version 4.0.2) was used for feature dimensionality reduction and construction of the radiomics score (Rad-Score). We followed a three-step procedure to identify robust radiomics features: (1) Feature reproducibility assessment using ICCs was established, and features with high stability (intraclass correlation coefficient >0.75) were retained for further analysis. (2) The high-stability radiomics features were subjected to Spearman's correlation analysis, with a correlation coefficient threshold of 0.75 (17). (3) We used the least absolute shrinkage and selection operator (LASSO) algorithm, with penalty parameter tuning conducted by 10-fold cross-validation, to select a suitable number of non-zero-weighted features. Rad-Score was calculated for each patient as a linear combination of selected features weighted by the respective nonzero coefficients.

The Rad-Score, combined with clinical and ultrasound factors, was incorporated into multivariate logistic regression to construct a radiomics nomogram.

Predictive performance and validation of clinical ultrasound nomogram, Rad-Score and radiomics nomogram

All models were validated using an internal validation cohort. The prediction performances of the clinical ultrasound nomogram, the Rad-Score and radiomics nomogram were evaluated by the area under the receiver operating characteristic curve (AUC) for both the training and internal

validation cohorts, and accuracy, sensitivity, specificity, negative predictive value (NPV), and positive predictive value (PPV) were calculated. A calibration curve was plotted to assess the calibration of the nomogram using the Hosmer-Lemeshow goodness-of-fit test. $P > 0.05$ indicated insignificant deviation from the theoretical perfect calibration. The clinical application value of the nomogram was determined through decision curve analysis (DCA) by quantifying the net benefit to the patient under different threshold probabilities.

Statistical analysis

All data were analyzed using the SPSS Statistics software version 23.0 (IBM, Armonk, NY, USA) and R software version 4.0.2 (<http://www.Rproject.org>).

An independent t-test was applicable to the continuous variables between groups, while a χ^2 test was used for the classification variables between groups. $P < 0.05$ was considered a statistically significant difference.

Results

Characteristics of the study cohorts

In this study, 216 GIST patients, comprising 98 with low-malignant potential and 118 with high-malignant potential, were enrolled. There were no significant differences in the distribution of clinical, ultrasound, and radiomics features between the low-malignant and high-malignant potential groups in the training and validation cohorts ($P > 0.05$) (Table 1). These results demonstrate the rationality of our training and validation cohort partitions.

Establishment and evaluation of clinical ultrasound nomogram

Univariate analysis of clinical and ultrasound parameters showed that there were no statistically significant differences in age, gender, BMI, internal echo, or growth pattern between low-

TABLE 1 Baseline Patient Characteristics.

Characteristics		Training cohort (n = 163)	Validation cohort (n = 53)	P- value
Patient demographics				
Sex	Male	95 (58.3)	31 (58.5)	0.979
	Female	68 (41.7)	22 (41.5)	
Age(mean \pm SD)		60 \pm 12	59 \pm 11	0.458
BMI(mean \pm SD)		23.2 \pm 3.1	23.0 \pm 3.4	0.787
Ultrasound features				
Tumor location	Gastric	116 (71.2)	35 (66.0)	0.480
	Extra-gastric	47 (28.8)	18 (34.0)	
Maximum diameter	≤ 5.0 cm	86 (52.8)	28 (52.8)	0.993
	> 5.0 cm	77 (47.2)	25 (47.2)	
The internal echo	Hypoecho	152 (93.3)	51 (96.2)	0.429
	Isoecho	11 (6.7)	2 (3.8)	
Echo homogeneity	Homogeneous	71 (43.6)	23 (43.4)	0.984
	Inhomogeneous	92 (56.4)	30 (56.6)	
Boundary	Clear	147 (90.2)	41 (77.4)	0.160
	Unclear	16 (9.8)	12 (22.6)	
Shape	Regular	77 (47.2)	25 (47.2)	1.0
	Irregular	86 (52.8)	28 (52.8)	
Necrotic cystic degeneration	Positive	66 (40.5)	20 (37.7)	0.722
	Negative	97 (59.5)	33 (62.3)	
Blood flow signals	Low blood supply	121 (74.2)	39 (73.6)	0.925
	Multiple blood supply	42 (25.8)	14 (26.4)	
Growth pattern	Endoluminal	82 (50.3)	28 (52.8)	0.750
	Exophytic	81 (49.7)	25 (47.2)	
Radiomics score*		0.51 (-0.77 to 1.12)	0.35 (-0.87 to 1.11)	0.612

Except where indicated, data are numbers of patients, with percentages in parentheses. SD: standard deviation.

*Data are presented as medians with interquartile ranges in parentheses.

$P < 0.05$ indicates that the difference is statistically significant.

malignant and high-malignant potential groups ($P > 0.05$). However, maximum diameter, tumor location, echo homogeneity, boundary, shape, necrotic cystic degeneration, and blood flow signals were statistically different ($P < 0.05$). These significant clinical and ultrasound features in the univariate analysis were included in the multivariate logistic regression to build a clinical ultrasound nomogram (Figure 7). Multivariate logistic regression analysis showed that the maximum tumor diameter (≤ 5.0 cm, > 5 cm) and echo homogeneity (both $P < 0.05$) were independent predictors of GIST risk, as shown in Table 2. The GIST risk prediction results are listed in Table 5. The AUC for the clinical ultrasound nomogram was 0.86 in the training cohort and 0.83 in the validation cohort (Figure 8).

Feature selection and radiomics score building

765 radiomics features were extracted. Using an ICC of 0.75 (for both intra and inter) as a cut-off for determining good reproducibility, 612 radiomics features with good reproducibility were selected for the subsequent assessment. After applying Spearman's correlation analysis (Figure 3), 68 features remained. Finally, the LASSO algorithm (Figure 4) with cross-validation was performed, and 16 radiomics features were used to develop the Rad-Score. The 16 selected radiomics features and the distribution of the corresponding risk coefficients are presented in Table 3. The Rad-Score was calculated using the following formula (18):

TABLE 2 Positive clinical and ultrasound factors of multivariate logistic regression analysis for GISTs.

Clinical and ultrasound factors	β	OR (95%CI)	P-value
Intercept	-2.48		
Maximum diameter	2.59	13.34 (6.03-31.59)	0.000
Echo homogeneity	1.01	2.73 (1.23-6.12)	0.000

95%CI, 95% confidence interval; OR, Odds ratio.

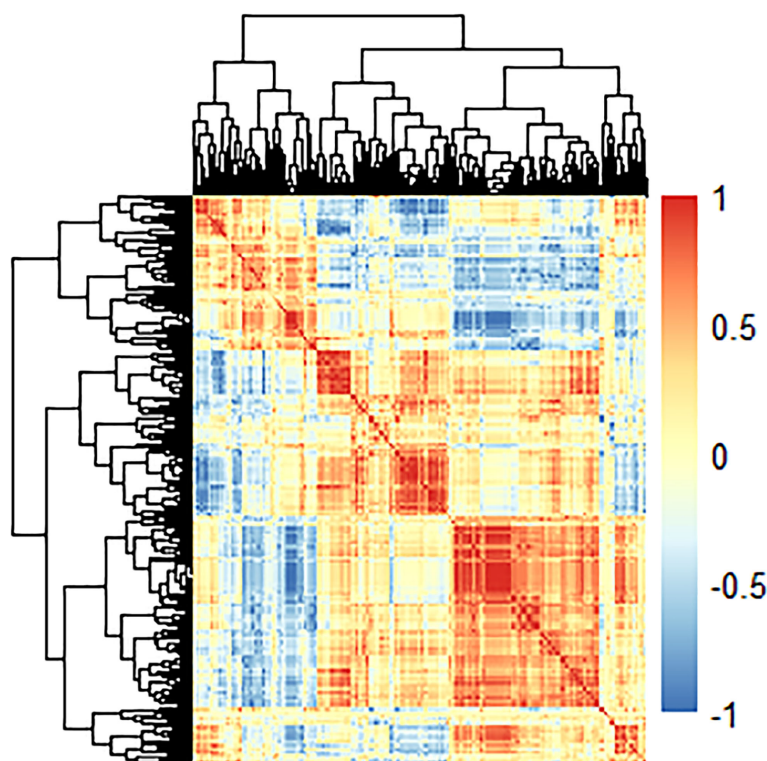
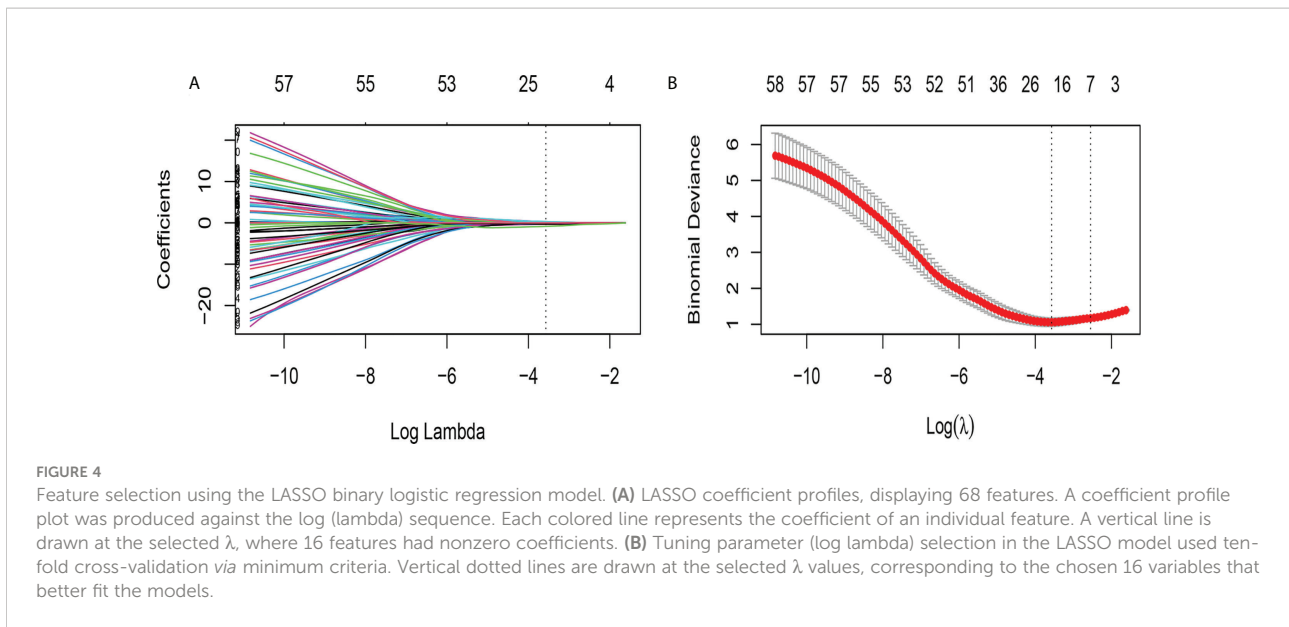


FIGURE 3

The heat-map displays the correlation between radiomics features in the training cohort.



$$\text{Radiomics score} = \sum_{i=1}^n \text{Coef}_i \times \chi_i$$

where Coef_i is the risk coefficient of each feature calculated by the LASSO model, and χ_i is the expression value of each feature, which refers to the 16 selected radiomics features in the present study. The cross-correlation matrices (Figure 5) showed that there were multiple complex cross-correlations among the 16 radiomics features, and Rad-Score indicated favorable prediction for discriminating the risk stratification of GIST (Figure 6).

There was a significant difference in Rad-Score between the low-malignant and high-malignant potential groups in both the training cohort (−0.696 VS 0.983, $P < 0.0001$) and the validation cohort (−0.650 vs. 0.952, $P < 0.0001$).

The prediction performance for discriminating the risk stratification of GIST of the Rad-score (AUC, 0.90 in the training cohort and 0.83 in the validation cohort) was not remarkable difference that of clinical ultrasound nomogram in the training cohort ($p=0.193$) and validation cohort ($p = 0.947$) (Table 5).

TABLE 3 Radiomics features and their coefficients that were included in the final assessment of GIST risk.

parameter		Coefficient
Feature1	original_shape2D_Sphericity	-0.37
Feature2	gradient_g lcm_Imc1	0.30
Feature3	logarithm_n gtdm_Strength	-0.29
Feature4	square_g lcm_Imc1	-0.23
Feature5	square_g lrlm_ShortRunLowGrayLevelEmphasis	0.25
Feature6	squareroot_g lcm_ClusterShade	-0.25
Feature7	wavelet.LH_g lcm_ClusterShade	-0.04
Feature8	wavelet.LH_g lcm_Correlation	-0.26
Feature9	wavelet.LH_g lcm_MCC	-0.04
Feature10	wavelet.LH_g ldm_DependenceVariance	-0.01
Feature11	wavelet.LH_g lszm_ZoneEntropy	0.29
Feature12	wavelet.HL_firstorder_Kurtosis	-0.06
Feature13	wavelet.HL_firstorder_Mean	-0.32
Feature14	wavelet.HL_g lcm_Imc2	-0.08
Feature15	wavelet.HL_g lcm_MCC	-0.10
Feature16	wavelet.HL_g ldm_SmallDependenceEmphasis	-0.85

TABLE 4 Variables and coefficients of the radiomics nomogram by multivariate logistic regression analysis.

Variable	β	OR (95%CI)	P-value
Intercept	-0.90		
Maximum diameter	1.88	6.57(2.54-18.0)	0.000
The Rad-Score	1.49	4.43(2.68-8.21)	0.000

95% CI, 95% confidence interval; OR, Odds ratio.

probability range for predicting the malignant potential of GISTs (Figure 9).

Discussion

As a rapidly developing discipline, radiomics is being increasingly used for clinical applications. Radiomics can extract feature data from digital medical images in a high-throughput manner, and this data can be quantitatively

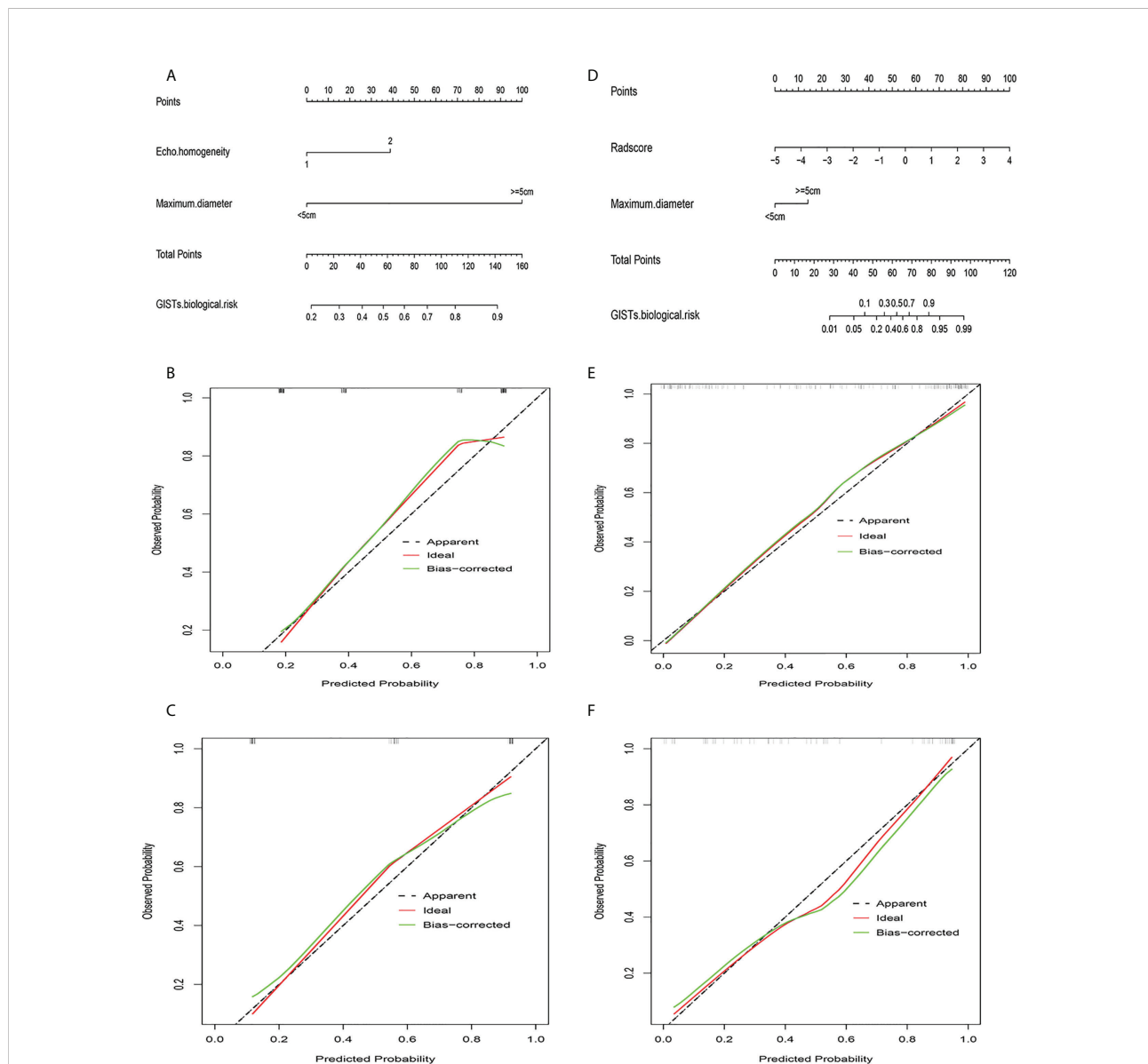


FIGURE 7 Clinical ultrasound nomogram and radiomics nomogram. (A) Nomogram of clinical ultrasound model. (B) Calibration curve of clinical ultrasound nomogram in training cohort. (C) Calibration curve of clinical ultrasound nomogram in validation cohort. (D) Nomogram of radiomics model. (E) Calibration curve of radiomics nomogram in training cohort. (F) Calibration curve of radiomics nomogram in validation cohort.

TABLE 5 Predictive performance of the radiomics nomogram compared with clinical ultrasound nomogram and the rad-score.

Model		AUC	Accuracy	Sensitivity	Specificity	PPV	NPV
Clinical ultrasound nomogram	training cohort	0.86	0.80	0.75	0.86	0.86	0.74
	validation cohort	0.83	0.83	0.88	0.79	0.84	0.82
The Rad-Score	training cohort	0.90	0.83	0.87	0.79	0.83	0.86
	validation cohort	0.83	0.79	0.90	0.57	0.74	0.81
radiomic nomogram	training cohort	0.92	0.84	0.84	0.85	0.87	0.81
	validation cohort	0.90	0.88	0.89	0.87	0.90	0.88

AUC, area under the receiver operating characteristic curve; PPV, positive predictive value; NPV, negative predictive value.

analyzed for the transformation of conventional clinical data into mineable high-dimensional quantitative feature data. In this study, radiomics features were combined with clinical and ultrasound image features to establish a radiomics-based nomogram for predicting the malignant potential of GISTs. Our results confirm that the radiomics nomogram has greater predictive power than the clinical ultrasound nomogram or the Rad-score for the malignant potential of GISTs and can guide clinical decision-making before surgery noninvasively and effectively.

According to previous studies, clinical and ultrasound features can help sonographers intuitively diagnose and predict the risk of GISTs (19, 20). Ultrasound imaging features mainly include the location, size, shape, growth pattern, internal echo, and cystic necrosis of the lesion (21). In this study, 12 variables of clinical and ultrasound signs were collected, and a clinical ultrasound model was established through univariate and multivariate logistic regression. Finally, two variables—tumor size and tumor echo homogeneity—were incorporated into the model, and a nomogram of the clinical ultrasound model was drawn. Tumor size is an important factor in evaluating the malignant potential and prognosis of GISTs. It is listed as a risk stratification index by the NIH grading system. The larger the tumor size, the higher the risk of infiltration

(22–24). Nevertheless, evaluating the malignancy of GISTs based on tumor size alone is insufficient. According to the NIH standards, the risk grade of GISTs is not only related to tumor size, but also to the mitotic index, tumor location, and whether or not the tumor is ruptured. Some small GISTs that are located in the intestine and possess high mitotic counts may be aggressive and have poor prognosis.

Echo homogeneity of GISTs is also an independent predictor of clinical ultrasound nomograms for evaluating the biological behavior of GISTs, which may be related to the fact that with increasing tumor malignancy, cystic degeneration and necrosis are more likely to occur inside the mass when the rate of differentiation and proliferation of tumor cells far exceeds the rate of proliferation of blood vessels (25, 26).

In ultrasonography, cystic degeneration and necrosis appear as an intratumoral inhomogeneous echogenicity. Previous studies (27–30) have shown that the presence of cystic degeneration and necrosis in the mass can be used as reliable indicators for GISTs malignancy evaluation, which is consistent with the results of our study. In this study, the AUC of the clinical ultrasound nomogram for predicting the malignant potential of GISTs was 0.86 in the training cohort and only 0.83 in the validation cohort. Although tumor size and echo homogeneity are important variables for predicting the risk

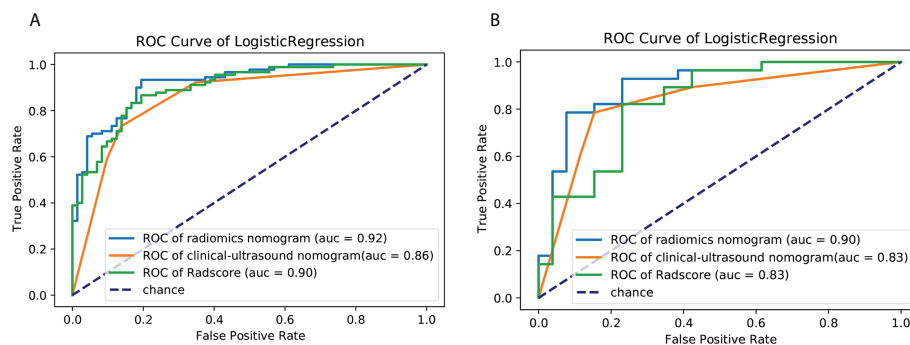
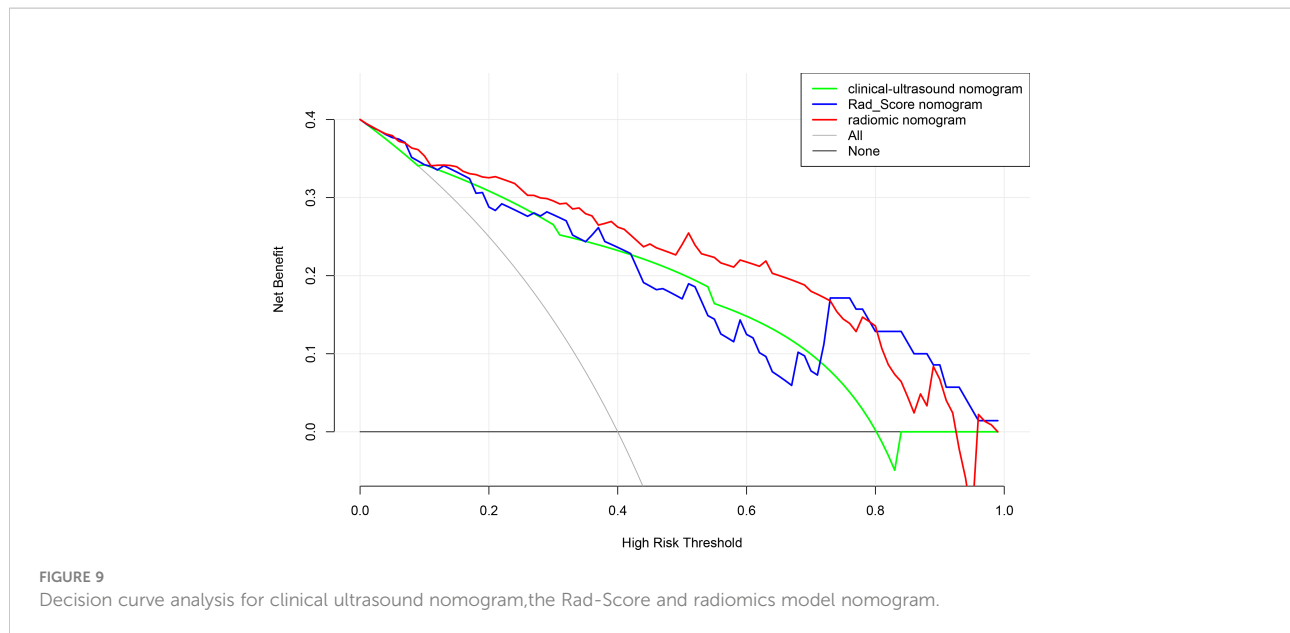


FIGURE 8

ROC curves of the clinical ultrasound nomogram, the Rad-Score and radiomics nomogram for predicting malignancy potential of GISTs in the (A) training cohort and (B) validation cohort. AUC, area under the receiver operating characteristic curve; GIST, gastrointestinal stromal tumor.



stratification of GISTs, they cannot fully reflect the inherent heterogeneity of GISTs and are easily affected by subjective factors and the professional level of sonographers.

Radiomics features extracted from ultrasound images can assess intratumor heterogeneity by quantifying tumor morphology, intensity, and texture features (31, 32), which could more effectively and objectively predict the malignant potential of GIST preoperatively. In this study, 765 radiomics features were extracted from ultrasound images using pyradiomics software. There was serious multicollinearity among the feature parameters. Features were extracted by the Spearman and LASSO algorithm methods to reduce overfitting. As a new feature selection method, Spearman and Lasso can achieve less redundancy and obtain more reliable radiomics features. The selected 16 radiomics features included one 2D shape-based feature, two first-order statistical features, and 13 texture features. These radiomics features represent an assessment of tumor shape and tumor heterogeneity (33).

Sphericity (measured as the shape of the ROI) is the ratio of the perimeter of the tumor region to the perimeter of a circle with the same surface area as the tumor region, which is correlated with the biological risk of GISTs. The first-order statistical features indicate that the image texture is disordered and complex, containing more information, and the pixel distribution is more random. High-order texture features reflect comprehensive information, such as space and distance, which can supplement the deficiencies of first-order statistical features (34). The radiomics features screened from GIST lesions in this study were significantly positively correlated with risk stratification (Figure 7), which indicates that high-malignant potential tumors have complex internal textures and random distributions. This hypothesis may be because of the fact that

high-malignant potential tumors are usually large, fast-growing, have insufficient blood supply to the central tissue, and are more prone to necrosis, rupture, and hemorrhage. Therefore, in our study, the Rad-Score based on multiple features was an important factor for assessing information regarding tumor heterogeneity.

When the Rad-Score was combined with clinical and ultrasound factors to incorporate multiple logistic regression, the results demonstrated that the tumor size and Rad-Score are independent predictors of the malignant potential of GISTs, thereby constructing a radiomics nomogram. Radiomics can quantitatively analyze the image characteristics and more accurately reflect tissue heterogeneity. The radiomics nomogram showed higher predictive performance (training cohort AUC: 0.92; validation cohort: 0.90) than the clinical ultrasound nomogram or the Rad-Score. In our retrospective data, 6 cases of high-malignant potential with tumor size less than 5 cm were accurately diagnosed using the radiomics nomogram, but they were underestimated by the clinical ultrasound nomogram. This suggests that our radiomics nomogram has better predictive performance in some cases with small tumor size. When the tumor size was larger than 5 cm, the total number of misclassifications in the clinical ultrasound nomogram remained higher than that in the radiomics nomogram. Therefore, the use of nomograms to further integrate radiomics features with these subjective clinical and ultrasound image features can lead to better diagnostic performance with good calibration. In this study, a radiomics-based nomogram provided a more accurate and personalized prediction for preoperative risk assessment of patients with GISTs by combining clinical and ultrasound risk factors. Additionally, the decision curves showed that the

radiomics nomogram was superior to the clinical ultrasound nomogram or the Rad-Score in terms of clinical validity, which confirmed the potential of the radiomics nomogram for broader clinical applications.

This study developed the first radiomics model based on 2D transabdominal ultrasound images to predict the risk stratification of GISTs. However, this study has some limitations. First, all data were obtained from a single center, and a multicenter study must be designed for further evaluation and validation. Second, this was a retrospective study, and selective bias could not be completely avoided. Third, we did not compare the feature extraction and dimensionality reduction algorithms, and the final feature selection may not be optimal, which may affect the predictive performance of the model.

Conclusion

As a noninvasive, non-radiation, and objective method, a radiomics nomogram based on radiomics features from 2D ultrasound and maximum tumor diameter was constructed for predicting malignant potential in GISTs, which could provide supplementary information for the prognostic evaluation of GISTs and guide patients to select the best treatment method minimizing their medical burden.

Data availability statement

The original contributions presented in the study are included in the article/supplementary material. Further inquiries can be directed to the corresponding author.

Ethics statement

The studies involving human participants were reviewed and approved by the ethics committee of Fujian Medical University Affiliated Union Hospital. Written informed consent for

participation was not required for this study in accordance with the national legislation and the institutional requirements.

Author contributions

ZC proposed the conception and design of this research and analyzed and interpreted the data. MZ and JG developed methodology. YT, XT, and QQ collected data and performed preprocessing. MZ, JG, and ZC were major contributors in writing the manuscript. All authors contributed to the article and approved the submitted version.

Funding

This work was supported by the 5th Round Joint Research Project from the Health and Family Planning commission and Education Department of Fujian Province of China under Grant (2019-WJ-06).

Conflict of interest

The authors declare that the research was conducted in the absence of any commercial or financial relationships that could be construed as a potential conflict of interest.

Publisher's note

All claims expressed in this article are solely those of the authors and do not necessarily represent those of their affiliated organizations, or those of the publisher, the editors and the reviewers. Any product that may be evaluated in this article, or claim that may be made by its manufacturer, is not guaranteed or endorsed by the publisher.

References

- Joensuu H, Hohenberger P, Corless CL. Gastrointestinal stromal tumour. *Lancet* (2013) 382:973–83. doi: 10.1016/s0140-6736(13)60106-3
- Miettinen M, Lasota J. Gastrointestinal stromal tumors - definition, clinical, histological, immunohistochemical, and molecular genetic features and differential diagnosis. *Virchows Archiv* (2001) 15:1–12. doi: 10.1007/s004280000338
- Nishida T, Blay J-Y, Hirota S, Kitagawa Y, Kang Y-K. The standard diagnosis, treatment, and follow-up of gastrointestinal stromal tumors based on guidelines. *Gastric Cancer* (2015) 15:3–14. doi: 10.1007/s10120-015-0526-8
- Dematteo RP, Heinrich MC, El-Rifai WM, Demetri G. Clinical management of gastrointestinal stromal tumors: before and after STI-571. *Hum Pathol* (2002) 33:466–77. doi: 10.1053/hupa.2002.124122
- Burkill GJC, Badran M, Al-Muderis O, Meirion Thomas J, Judson IR, Fisher C, et al. Malignant gastrointestinal stromal tumor: Distribution, imaging features, and pattern of metastatic spread. *Radiology* (2003) 226:527–32. doi: 10.1148/radiol.2262011880
- Maldonado FJ, Sheedy SP, Iyer VR, Hansel SL, Bruining DH, Mccollough CH, et al. Reproducible imaging features of biologically aggressive gastrointestinal stromal tumors of the small bowel. *Abdom Radiol* (2017) 43:1567–74. doi: 10.1007/s00261-017-1370-6
- Peng Y, Lin P, Wu L, Wan D, Zhao Y, Liang L, et al. Ultrasound-based radiomics analysis for preoperatively predicting different histopathological subtypes of primary liver cancer. *Front Oncol* (2020) 24:1646. doi: 10.3389/fonc.2020.01646

8. Xiong L, Chen H, Tang X, Chen B, Jiang X, Liu L, et al. Ultrasound-based radiomics analysis for predicting disease-free survival of invasive breast cancer. *Front Oncol* (2021) 11:621993. doi: 10.3389/fonc.2021.621993
9. van Timmeren JE, Cester D, Tanadini-Lang S, Alkadhi H, Baessler B. Radiomics in medical imaging—"how-to" guide and critical reflection. *Insights Imaging* (2020) 11:91. doi: 10.1186/s13244-020-00887-2
10. Gillies RJ, Kinahan PE, Hricak H. Radiomics: Images are more than pictures, they are data. *Radiology* (2016) 278:563–77. doi: 10.1148/radiol.2015151169
11. Ren C, Wang S, Zhang S. Development and validation of a nomogram based on CT images and 3D texture analysis for preoperative prediction of the malignant potential in gastrointestinal stromal tumors. *Cancer Imaging* (2020) 20:5. doi: 10.1186/s40644-019-0284-7
12. Chen T, Ning Z, Xu L, Feng X, Han S, Roth HR, et al. Radiomics nomogram for predicting the malignant potential of gastrointestinal stromal tumours preoperatively. *Eur Radiol* (2018) 29:1074–82. doi: 10.1007/s00330-018-5629-2
13. Song Y, Li J, Wang H, Liu B, Yuan C, Liu H, et al. Radiomics nomogram based on contrast-enhanced CT to predict the malignant potential of gastrointestinal stromal tumor: A two-center study. *Acad Radiol* (2021) 5:S1076–6332(21)00220-8. doi: 10.1016/j.acra.2021.05.005
14. Mao H, Zhang B, Zou M, Huang Y, Yang L, Wang C, et al. MRI-Based radiomics models for predicting risk classification of gastrointestinal stromal tumors. *Front Oncol* (2021) 11:631927. doi: 10.3389/fonc.2021.631927
15. Liu B, Liu H, Zhang L, Song Y, Yang S, Zheng Z, et al. Value of contrast-enhanced CT based radiomic machine learning algorithm in differentiating gastrointestinal stromal tumors with KIT exon 11 mutation: a two-center study. *Diagn Interv Radiol* (2022) 28:29–38. doi: 10.5152/dir.2021.21600
16. Sauerbrei W, Boulesteix AL, Binder H. Stability investigations of multivariable regression models derived from low- and high-dimensional data. *J Biopharmaceutical Stat* (2011) 21:1206–31. doi: 10.1080/10543406.2011.629890
17. Hazra A, Gogtay N. Biostatistics series module 6: Correlation and linear regression. *Indian J Dermatol* (2016) 61:593–601. doi: 10.4103/0019-5154.193662
18. Yao F, Ding J, Hu Z, Cai M, Liu J, Huang X, et al. Ultrasound-based radiomics score: a potential biomarker for the prediction of progression-free survival in ovarian epithelial cancer. *Abdominal Radiol* (2021) 46:4936–45. doi: 10.1007/s00261-021-03163-z
19. Liu S, Pan X, Liu R, Zheng H, Chen L, Guan W, et al. Texture analysis of CT images in predicting malignancy risk of gastrointestinal stromal tumours. *Clin Radiol* (2018) 73:266–74. doi: 10.1016/j.crad.2017.09.003
20. Sugihara T, Koda M, Tanimura T, Yoshida M, Murawaki Y. A report of three cases of exophytic gastrointestinal stromal tumor detected by transabdominal ultrasound. *J Med Ultrason* (2001) (2016) 43:107–11. doi: 10.1007/s10396-015-0661-1
21. Dematteo RP, Gold JS, Saran L, Gönen M, Liau KH, Maki RG, et al. Tumor mitotic rate, size, and location independently predict recurrence after resection of primary gastrointestinal stromal tumor (GIST). *Cancer* (2008) 112:608–15. doi: 10.1002/cncr.23199
22. Joensuu H. Risk stratification of patients diagnosed with gastrointestinal stromal tumor. *Hum Pathol* (2008) 39:1411–9. doi: 10.1016/j.humpath.2008.06.025
23. Gronchi A. Risk stratification models and mutational analysis: keys to optimising adjuvant therapy in patients with gastrointestinal stromal tumour. *Eur J Cancer* (2013) 49:884–92. doi: 10.1016/j.ejca.2012.10.025
24. Wang C, Li H, Jiaerken Y, Huang P, Sun L, Dong F, et al. Building CT radiomics-based models for preoperatively predicting malignant potential and mitotic count of gastrointestinal stromal tumors. *Transl Oncol* (2019) 12:1229–36. doi: 10.1016/j.tranon.2019.06.005
25. Li J, Ye Y, Wang J, Zhang B, Qin S, Shi Y, et al. Chinese Consensus guidelines for diagnosis and management of gastrointestinal stromal tumor. *Chin J Cancer Res* (2017) 29:281–93. doi: 10.21147/j.issn.1000-9604.2017.04.01
26. Ren C, Wang S, Zhang S. Development and validation of a nomogram based on CT images and 3D texture analysis for preoperative prediction of the malignant potential in gastrointestinal stromal tumors. *Cancer Imaging* (2020) 20:5. doi: 10.1186/s40644-019-0284-7
27. Ulasan S, Koc Z, Kayaselcuk F. Gastrointestinal stromal tumours: CT findings. *Br J Radiol* (2008) 81:618–23. doi: 10.1259/bjr/90134736
28. Chen T, Xu L, Dong X, Li Y, Yu J, Xiong W, et al. The roles of CT and EUS in the preoperative evaluation of gastric gastrointestinal stromal tumors larger than 2 cm. *Eur Radiol* (2019) 29:2481–9. doi: 10.1007/s00330-018-5945-6
29. Shao M, Niu Z, He L, Fang Z, He J, Xie Z, et al. Building radiomics models based on triple-phase CT images combining clinical features for discriminating the risk rating in gastrointestinal stromal tumors. *Front Oncol* (2021) 11:737302. doi: 10.3389/fonc.2021.737302
30. Takahashi K, Nihei T, Aoki Y, Konno N, Nakagawa M, Munakata A, et al. Gastric gastrointestinal stromal tumor with predominant cystic formation diagnosed by endoscopic ultrasound-fine needle aspiration. *Clin J Gastroenterol* (2020) 13:359–64. doi: 10.1007/s12328-019-01058-7
31. Zhang QW, Zhou XX, Zhang RY, Chen SL, Liu Q, Wang J, et al. Comparison of malignancy-prediction efficiency between contrast and non-contrast CT-based radiomics features in gastrointestinal stromal tumors: A multicenter study. *Clin Transl Med* (2020) 10:e291. doi: 10.1002/ctm2.91
32. Feng C, Lu F, Shen Y, Li A, Yu H, Tang H, et al. Tumor heterogeneity in gastrointestinal stromal tumors of the small bowel: volumetric CT texture analysis as a potential biomarker for risk stratification. *Cancer Imaging* (2018) 18:46. doi: 10.1186/s40644-018-0182-4
33. Ganeshan B, Panayiotou E, Burnand K, Dizdarevic S, Miles K. Tumour heterogeneity in non-small cell lung carcinoma assessed by CT texture analysis: A potential marker of survival. *Eur Radiol* (2012) 22:796–802. doi: 10.1007/s00330-011-2319-8
34. Szczypiński PM, Strzelecki M, Materka A, Klepaczko A. MaZda: a software package for image texture analysis. *Comput Methods Progr BioMed* (2009) 94:66–76. doi: 10.1016/j.cmpb.2008.08.005